Title

Topographic Variation of Retinal Vascular Density in Normal Eyes Using Optical Coherence Tomography Angiography

Journal

Translational Vision Science & Technology, 10(12)

ISSN

2164-2591

Authors

Park, Michael M
Young, Benjamin K
Shen, Liangbo L
et al.

Publication Date

2021-10-14

DOI

10.1167/tvst.10.12.15

Peer reviewed

tvst

Article

Topographic Variation of Retinal Vascular Density in Normal Eyes Using Optical Coherence Tomography Angiography

Michael M. Park[1], Benjamin K. Young[1], Liangbo L. Shen[1], Ron A. Adelman[1], and Lucian V. Del Priore[1]

[1] Department of Ophthalmology and Visual Science, Yale University School of Medicine, New Haven, CT, USA

Correspondence: Lucian V. Del Priore, Department of Ophthalmology and Visual Science, Yale University School of Medicine, 40 Temple Street, Suite 1B, New Haven, CT 06510, USA.
e-mail: lucian.delpriore@yale.edu

Received: August 19, 2020
Accepted: September 10, 2021
Published: October 14, 2021

Keywords: optical coherence tomography angiography; normative database; vessel density topography; normal

Citation: Park MM, Young BK, Shen LL, Adelman RA, Del Priore LV. Topographic variation of retinal vascular density in normal eyes using optical coherence tomography angiography. Transl Vis Sci Technol. 2021;10(12):15, https://doi.org/10.1167/tvst.10.12.15

Purpose: To establish a continuous topography of retinal vessel density in normal eyes using optical coherence tomography angiography (OCTA).

Methods: A retrospective chart review was performed, and 8-mm × 8-mm OCTA images from 22 normal eyes were analyzed. Vessel density was plotted as a continuous function of distance from the foveal center (radial vessel density) and directional meridians (directional vessel density) for the superficial capillary plexus and deep capillary plexus.

Results: Continuous radial and directional vessel density plots for the superficial and deep capillary plexus were generated. Radial vessel density analysis revealed transition points at 657 microns (95% confidence interval [CI], 619–696) and 950 microns (95% CI, 903–997) from the foveal center for the superficial plexus and deep plexus, respectively. Directional vessel density analysis demonstrated significant vessel density variations in these vascular layers and provided greater detail compared to traditional quadrant analysis.

Conclusions: There are significant topographic variations of retinal vessel density in normal eyes. Continuous vessel density analysis offers greater sensitivity in detecting topographic vessel density changes compared to traditional methods of analysis.

Translational Relevance: This study establishes a normative continuous vessel density topography that may help elucidate the role of the vascular bed in different chorioretinal diseases.

Introduction

The neurosensory retina has a dual blood supply composed of the retinal and choroidal vasculature that supply the inner and outer layers of the retina, respectively. Each vascular supply exhibits its own characteristic pattern. For example, the retinal vasculature does not supply the center of the macula, known as the foveal avascular zone. The blood supply to this region is dependent on the choroidal vasculature.[1] Many retinal diseases follow characteristic topographic patterns that are specific for individual diseases. For example, sickle cell retinopathy leads to peripheral ischemia and is accompanied by irregular enlargement of the foveal avascular zone and focal macular thinning without significant changes in the choriocapillaris.[2,3] Bull's-eye maculopathy due to hydroxychloroquine toxicity is known to affect the parafovea in its early stages.[4] While the exact pathophysiology of many diseases is not fully understood, some of the different topographic patterns may be attributable to the differences in structural topographic density of cells, including the retinal and choroidal vasculature.

For decades, fluorescein angiography and indocyanine green angiography have been the gold standard for imaging the retinal and choroidal vasculature.[5] However, these modalities are unable to distinguish between the different vascular layers within the retina, as the captured images do not contain resolved depth information. Optical coherence tomography angiography (OCTA) is a noninvasive imaging modality that allows segmentation of the individual vascular layers, including the superficial vascular plexus, deep vascular

plexus, and choriocapillaris. OCTA has become widely used by clinicians and researchers to describe the posterior segment vasculature in normal eyes and eyes with chorioretinal pathology, such as diabetic retinopathy, age-related macular degeneration, and retinal artery and vein occlusions.[6–13]

Previous OCTA studies have demonstrated that chorioretinal diseases such as diabetic retinopathy and macular degeneration are associated with decreased vessel density compared to normal eyes.[6,7,13] These studies compare the average vessel density of entire maculae and do not report vessel density variation within the macula. A few studies have illustrated that there are regional differences in the retinal vessel density in normal eyes, particularly at different discrete parafoveal quadrants of the macula.[9,14,15] However, these prior analyses were performed on discrete sectors of the macula. A continuous analysis of topographic variations in retinal vessel density has not yet been well characterized. In the present study, we use high-resolution OCTA images of normal eyes to establish the continuous topographic variations of vessel density at the superficial and deep capillary plexus.

Methods

A retrospective chart review was performed on patients who had undergone OCTA imaging as part of their care at the Yale Eye Center between April 2018 and January 2020. This study was approved by the Yale University Institutional Review Board, and informed consent was waived for this retrospective chart review. The study was conducted in accordance with the tenets of the Declaration of Helsinki.

The 8-mm × 8-mm OCTA images of normal eyes were included for the analysis (Fig. 1). Inclusion criteria included a normal anterior segment examination, normal dilated fundus examination, normal OCT B-scan, and visual acuity of 20/25 or better. Patients with a normal eye examination with visual symptoms that could not be explained were excluded from the study. Eyes that had undergone ocular surgery, including cataract surgery, or had documented disease, including chorioretinal disease, optic neuropathy, or glaucoma, were excluded. Patients with systemic hypertension or diabetes without documented hypertensive or diabetic retinopathy were not excluded from the study. Eyes with poor-quality images on OCTA due to eye movements or media opacities, indicated by signal strength of less than 6/10, were excluded.

All OCTA images had been obtained using the Zeiss Cirrus HD-OCT 5000 with Angioplex (Zeiss Meditec, Dublin, CA, USA). The device has an A-scan rate of 68,000 scans per second and light source with a central wavelength of 840 nm, with an A-scan depth of 2.0 mm in tissue, axial resolution of 5 microns, and transverse resolution of 15 microns. These images are generated using the OCT-microangiography complex algorithm. The OCTA device also incorporates a retinal-tracking

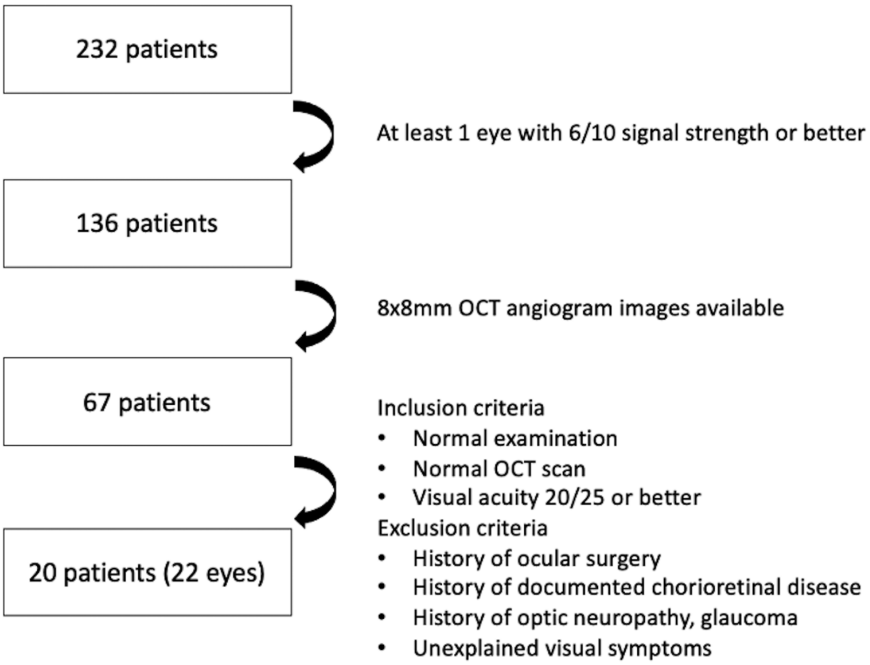

Figure 1. OCTA image selection. OCTA images from 22 normal eyes from 20 patients were included for the study.

technology to achieve three-dimensional en face angiographic images that have minimal movement artifacts. En face 8-mm × 8-mm OCTA images of the superficial plexus, deep plexus, and choriocapillaris were analyzed for the study. Automatic built-in retinal segmentation was used to segment the superficial capillary plexus from the inner limiting membrane to the inner plexiform layer and the deep capillary plexus from the inner nuclear layer to the outer plexiform layer.[16] All images were exported in 1024 × 1024 pixel resolution.

Imaging Processing

The foveal avascular zone was manually outlined on the en face OCTA images at the superficial and deep layers by two independent graders (MMP, BKY) using ImageJ (National Institutes of Health, Bethesda, MD, USA) as previously described.[7,11,14,17] The foveal avascular zone was used to identify the foveal center for each eye. Images were binarized using the local threshold Phansalkar method set to a radius of

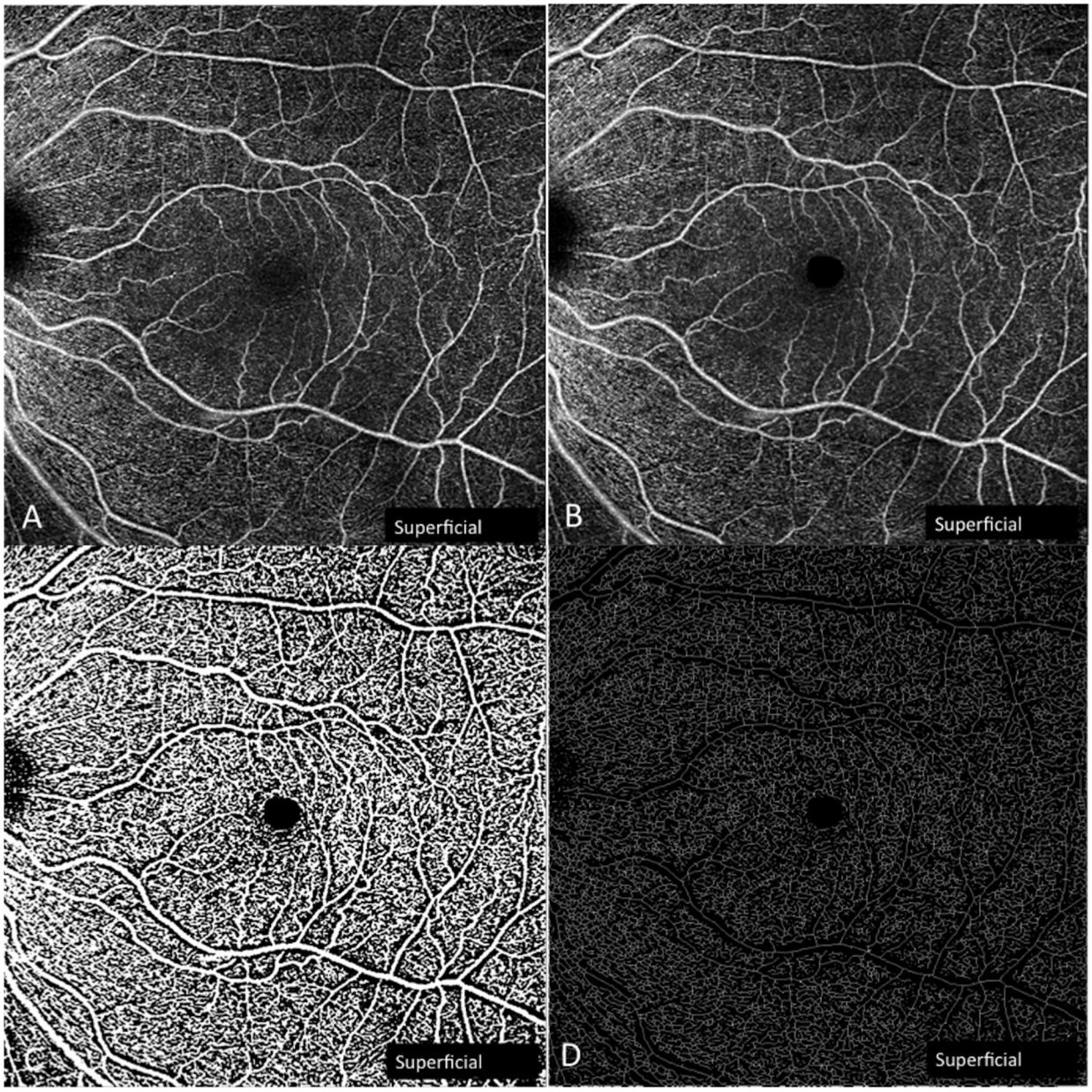

Figure 2. Imaging processing. (**A**) The 8-mm × 8-mm en face OCTA of a normal eye at the superficial capillary plexus. (**B**) The foveal avascular zone has been manually determined. (**C**) The image has been binarized using the local Phansalkar method, which depicts each pixel as black or white. (**D**) The image has been binarized and skeletonized, reducing each vessel into a single pixel in diameter regardless of the vessel diameter.

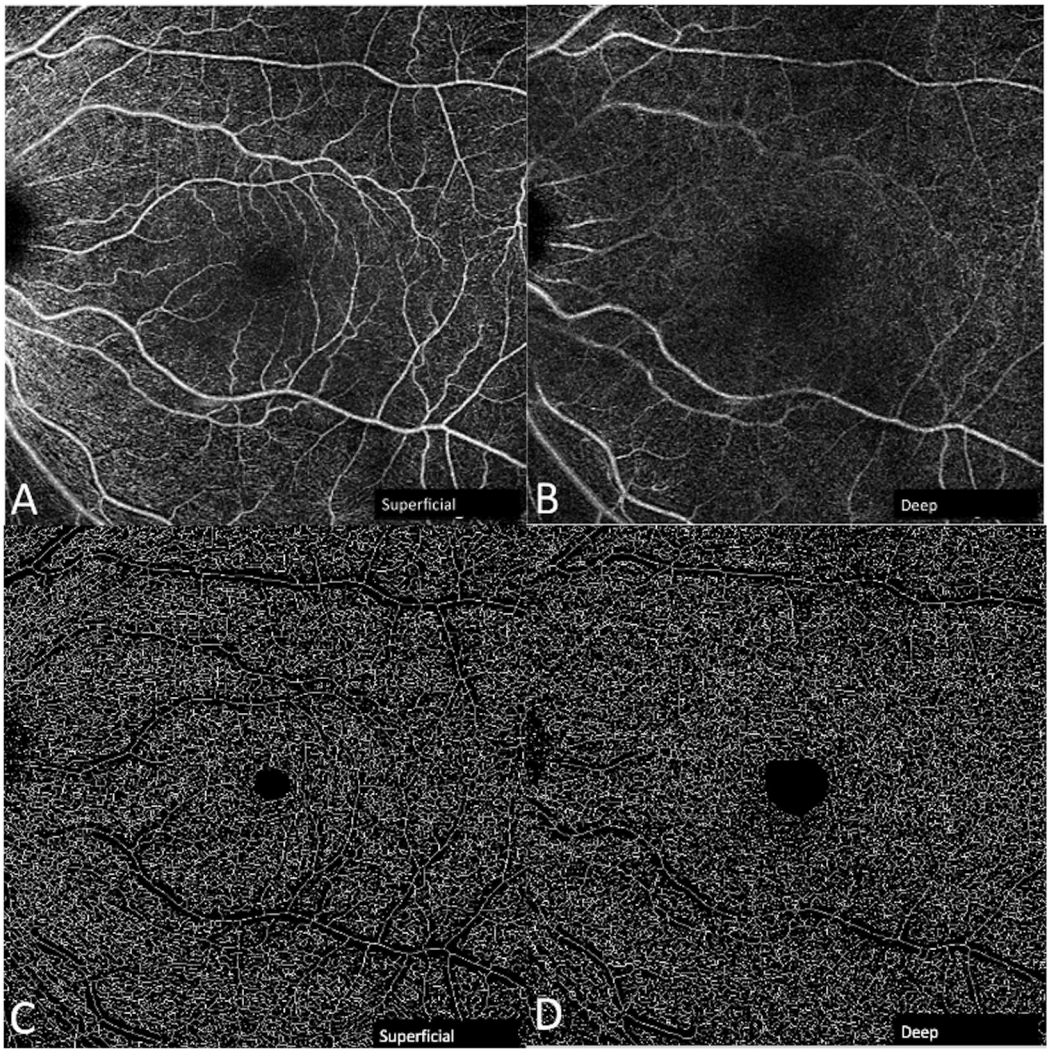

Figure 3. The 8-mm × 8-mm en face OCTA layer segmentation. OCTA provides segmentation of the (**A**) superficial capillary plexus and (**B**) deep capillary plexus. The images have been processed for the (**C**) superficial plexus and (**D**) deep plexus.

15 pixels, as previously reported, to control for variations in illuminations or contrast within the image.[17–21] The binarized images were then skeletonized to convert all vessels into a single pixel diameter, regardless of the original vessel caliber. This skeletonization step ensured that the larger-caliber vessels, which do not play a significant role in gas exchange, do not overestimate vessel density in the analysis.[11] Imaging processing is summarized in Figure 2. OCTA images at the superficial and deep plexus for one representative eye, before and after processing, are shown in Figure 3.

Vessel Density

Vessel density was defined as the percentage of a given area that was occupied by blood vessels. As blood vessels are depicted on binarized and skeletonized images as white pixels, vessel density was calculated from these images by taking the ratio of white pixels to total pixels in an area. The vessel density in concentric rings around the foveal center was calculated (Fig. 4). Each concentric ring was exactly 1 pixel in radius larger than the previous. Vessel density at progressively larger concentric rings was calculated until an edge of the image was met. In this fashion, a continuous radial vessel density plot as a function of pixels away from the foveal center was generated. Pixels were then converted to microns, as each image was exactly 1024 pixels and 8 mm in width. Radial analysis for the superficial and deep capillary plexus began from 300 microns away from the foveal center to minimize the inherent noise around the foveal avascular zone in OCTA images. Vessel density was then replotted as a percentage of each individual eye's maximum vessel density, and these

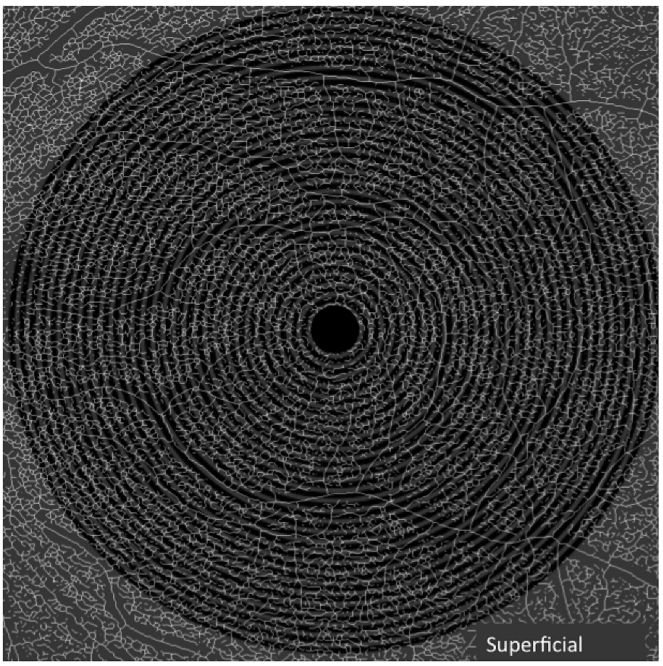

Figure 4. Schematic of radial continuous vessel density analysis. A binarized, skeletonized OCTA image is depicted with alternating *gray* and *black* concentric rings. The vessel density in each concentric ring was calculated. Each ring was exactly 1 pixel larger than the previous ring, in order to create a radial vessel density topography map as a continuous function of distance from the foveal center. Rings shown are greater than 1 pixel apart for illustration purposes. Radial analysis for the superficial and deep capillary plexus began from 300 microns away from the foveal center.

normalized vessel density plots were used to create an average continuous radial vessel density plot for each vascular layer. These continuous radial plots were generated using Python 3.7 (Python Software Foundation, Wilmington, DE, USA). MatPlotLib and NumPy library software were used in conjunction with Python for visualization of data and calculation of 95% confidence intervals (CIs), respectively.

The vessel density along different directional meridians was also calculated. Images were converted to polar coordinates using Python 3.7 and Scikit-Learn library tools (French Institute for Research in Computer Science and Automation, Rocquencourt, France). Vessel density along a linear vector extending from the foveal center toward the nasal periphery, designated as the 0-degree meridian, was calculated. This process was repeated at every 1-degree meridian for 360 degrees around the foveal center, where 90 degrees represents the superior meridian, 180 degrees temporal, and 270 degrees inferior (Fig. 5). The normalized directional vessel density plots were used to create a mean continuous directional vessel density plot for each vascular layer. The average vessel density of the nasal, superior, temporal, and inferior quadrants was then calculated for each vascular layer.

Statistical Analysis

A segmented mixed regression analysis was performed on the continuous radial plots to identify the vessel density transition points for the superficial plexus and deep capillary plexus.[22] A repeated-measures analysis of variance with the Geisser–Greenhouse correction to adjust for deviation from sphericity and Tukey's multiple comparisons test were used to compare the mean vessel density between quadrants. A P value <0.05 was considered statistically significant. A sensitivity analysis was performed by removing one eye at a time from the statistical analysis to evaluate for any outliers in the sample. All statistical analysis was performed with Prism v8.0 (GraphPad Software, San Diego, CA, USA).

Results

The 8-mm × 8 mm OCTA images from 22 normal eyes from 20 patients (45% male) were included for this analysis. Eighteen patients in the cohort had documented ocular pathology or unexplained visual symptoms in the fellow eye. Two patients had two eyes that met inclusion criteria. The average patient age in this cohort was 44.3 ± 15.1 years (range, 18–63 years).

Vessel density as a continuous function of distance from the foveal center was plotted for the superficial and deep plexus (Fig. 6). A segmented mixed regression analysis revealed a statistically significant transition point at both vascular layers (Supplementary Fig. S1). The transition point occurred at 657 microns from the foveal center (95% CI, 619–696 microns; $P < 0.001$ between slopes of two phases) for the superficial plexus and 950 microns (95% CI, 903–997 microns; $P < 0.001$ between slopes of two phases) for the deep plexus (Fig. 7).

Vessel density as a function of directional meridians was plotted for the superficial and deep plexus (Fig. 8). These plots revealed significant directional vessel density variability within each vascular layer. Vessel density was greatest along the 25-degree meridian in the superficial plexus and lowest in the 280-degree meridian in the deep plexus. Average vessel densities at the nasal, superior, temporal, and inferior quadrants were then generated for supplemental analysis (Fig. 9). In the quadrant analysis of the superficial plexus, the nasal quadrant had the greatest vessel density ($P < 0.0001$), and the superior quadrant

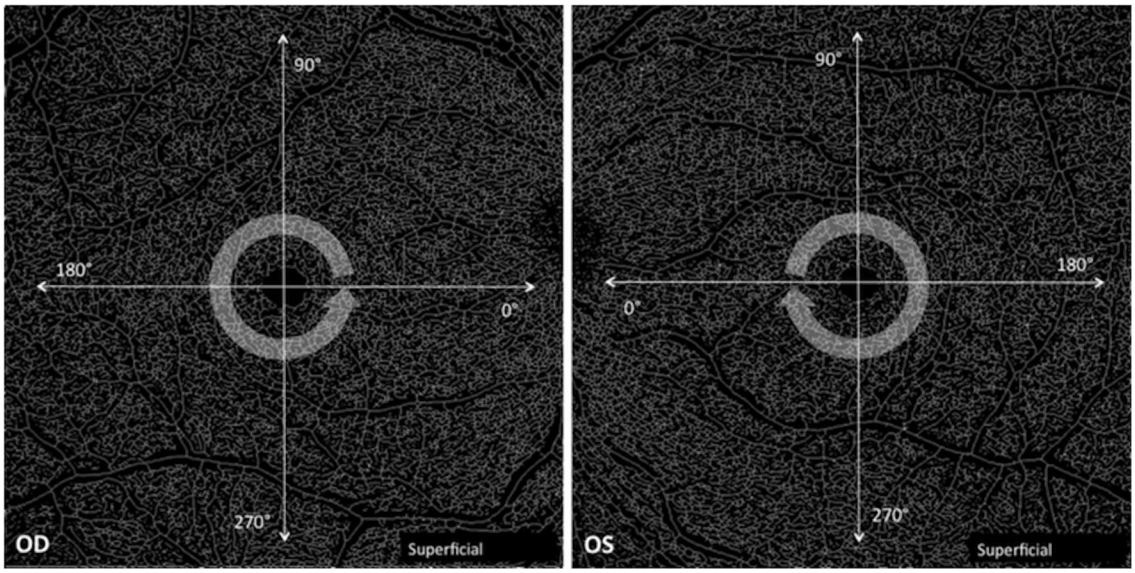

Figure 5. Schematic of directional continuous vessel density analysis. A binarized, skeletonized image is shown with a linear vector extending in different meridians from the foveal center (*thin arrows*). The vessel density along this linear vector was calculated and repeated at each 1-degree meridian for 360 degrees around the foveal center (*thick arrows*). Zero degrees corresponds to nasal meridian, 90 degrees superior, 180 degrees temporal, and 270 degrees inferior, for both the right and left eyes.

had greater vessel density compared to the temporal ($P = 0.0003$) and inferior quadrants ($P < 0.0001$). In the deep plexus, the nasal, superior, and temporal quadrants had greater vessel density compared to the inferior quadrant ($P < 0.0124$). A sensitivity analysis was performed removing one eye at a time and confirmed these quadrant relationships remained consistent.

Discussion

OCTA is a useful imaging technique that allows reliable, noninvasive, three-dimensional imaging of the retinal microvasculature. It allows for segmentation of individual layers of the posterior vasculature, which is not available on standard fluorescein and indocyanine green angiography.[23,24] OCTA is widely used to calculate vessel density in these different vascular layers in both normal eyes and eyes with chorioretinal pathology. Prior studies have identified regional differences in vessel density in normal eyes, particularly in the different parafoveal regions.[9,14,15] To the best of our knowledge, a continuous topographic analysis of the retinal vasculature has not yet been performed.

Radial Vessel Density Analysis

Our radial vessel density analysis at the superficial and deep capillary plexus demonstrates a sharp increase in vessel density followed by a plateau at a specific distance away from the foveal center. We determined that this transition point occurs at approximately 657 microns from the foveal center at the superficial plexus and 950 microns at the deep plexus. Interestingly, the identified transition points occur beyond the edge of the foveal avascular zone, which has been cited to have a radius of 250 to 350 microns for the superficial capillary plexus and 300 to 450 microns for the deep plexus on previous OCTA studies.[11,14,25] Our study suggests that the superficial and deep capillary plexus are not homogeneous networks of vessels beyond the foveal avascular zone, as was previously suggested. Gadde et al.[14] found that there was no difference in the vessel density in three concentric rings of increasing diameter around the foveal avascular zone in both the superficial and deep capillary plexus of normal eyes. It is important to note that the rings used in the analysis by Gadde et al.[14] were each 250 microns wide, whereas the present study uses much smaller rings that are approximately 8 microns wide, offering greater sensitivity to vessel density changes. Further studies are needed to determine the clinical significance of these identified transition points at the superficial and deep capillary plexus and what role they may have in the pathogenesis of various chorioretinal diseases.

Directional Vessel Density Analysis

Prior studies evaluating the directional differences in vessel density have compared the vessel density at

the superior, inferior, nasal, and temporal quadrants of the macula.[9,14] Our directional vessel density plots offer a novel way to report vessel density as a continuous function of directional meridians, which is more precise than traditional quadrant analysis. In our analysis, we demonstrate that the superficial plexus has the greatest vessel density along the superonasal meridian, and the deep plexus has the lowest vessel density along the inferonasal meridian. These findings raise interesting questions about the utility of

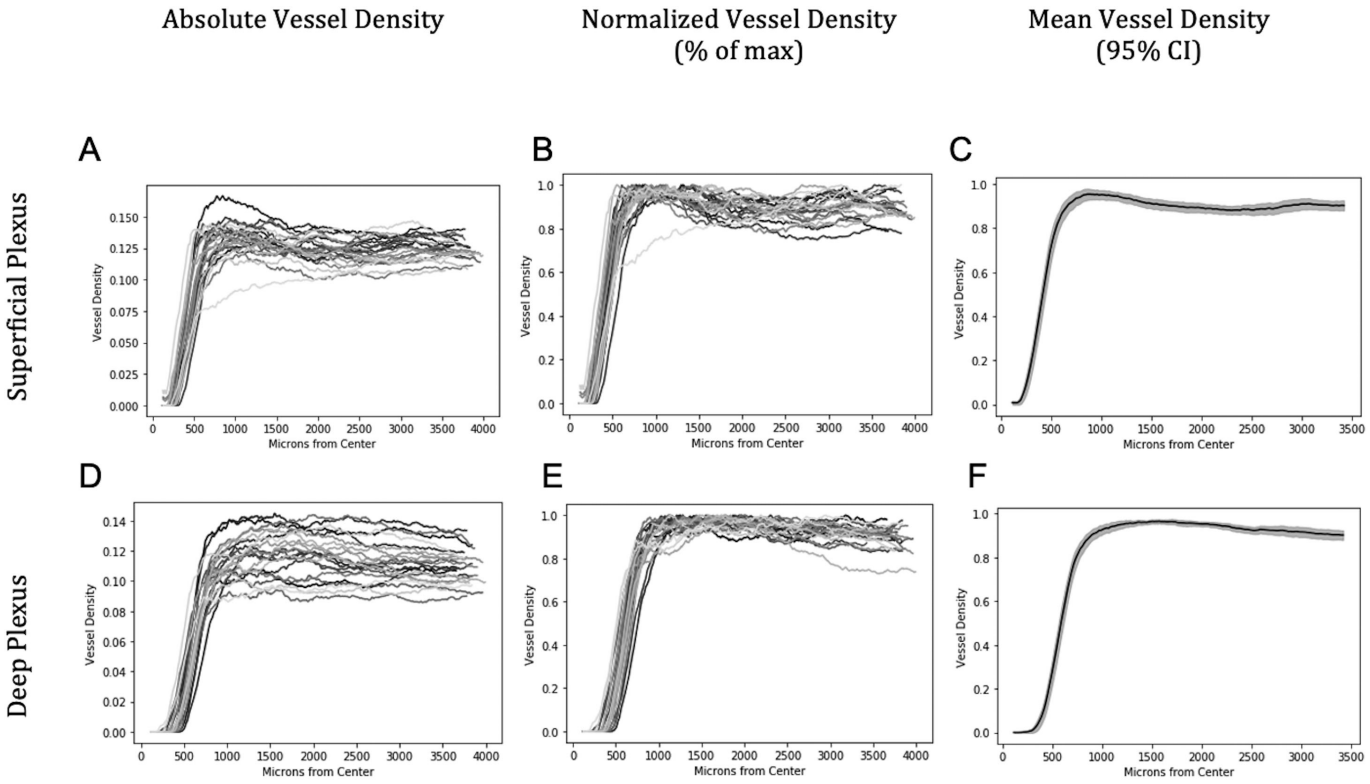

Figure 6. Continuous radial vessel density plots. Radial vessel density curves were generated using binarized and skeletonized OCTA images for the superficial plexus (*top row*) and deep plexus (*bottom row*). (*Left*) Absolute vessel density is plotted as a function of distance from the foveal center for 22 eyes. (*Middle*) Vessel density curves were normalized as a percentage of each eye's maximum vessel density. (*Right*) Mean vessel density plots are shown with a 95% CI.

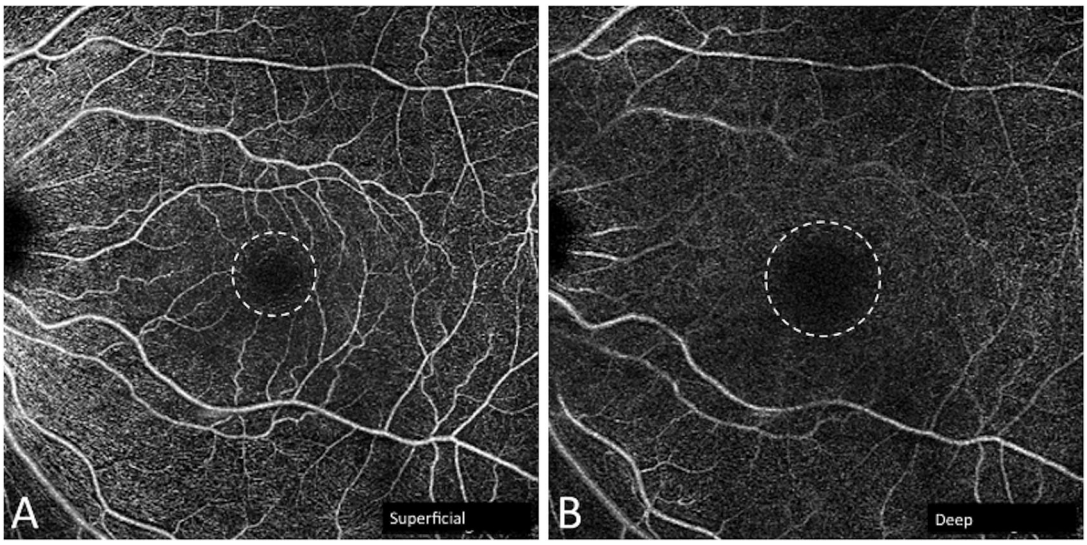

Figure 7. (**A**) The superficial plexus has a transition point at 657 microns from the foveal center. (**B**) The deep plexus has a transition point at 950 microns. The mean transition points are outlined in each vascular layer (*broken white lines*).

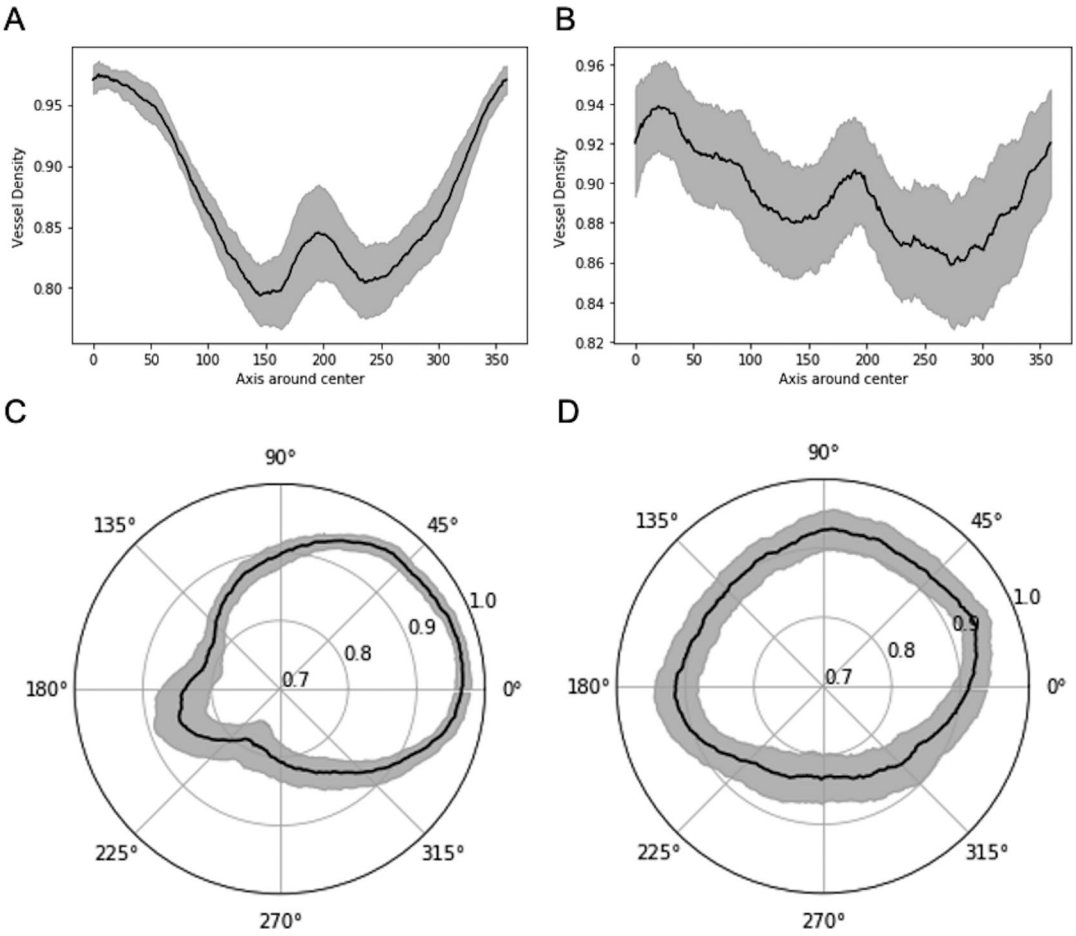

Figure 8. Continuous directional vessel density plots. Directional vessel density plots were generated using binarized and skeletonized OCTA images. Vessel density was plotted as a function of directional meridians as linear plots (*top*) and polar plots (*bottom*). Zero degrees represents the nasal meridian, 90 degrees superior, 180 degrees temporal, and 270 inferior. The mean vessel density with a 95% CI is shown at the superficial plexus (**A**, **C**) and deep plexus (**B**, **D**).

traditional quadrant analyses and may suggest that spatial differences in vessel density may be more accurately represented by analyzing the superonasal, superotemporal, inferotemporal, and inferonasal quadrants. Our continuous analysis is also able to detect subtle vessel density fluctuations that quadrant analysis cannot detect. For example, our continuous analysis revealed a small, relative vessel density peak inferotemporally along the 200-degree meridian at both the superficial and deep plexus. These smaller vessel density peaks were lost when we performed the traditional quadrant analysis. We advocate for the use of continuous vessel density plots as adjuncts to quadrant analysis in future studies. This concept is already widely employed in glaucoma, where the retinal nerve fiber thickness is reported not just in quadrants but also as a continuous, directional nerve fiber thickness plot. It is likely that continuous plots will be more sensitive at detecting early changes in the vascular bed for each of the three layers as disease develops.

Interestingly, our quadrant analysis of the superficial and deep capillary plexus differed from prior studies that reported greater vessel density in the superior and inferior macula compared to the nasal and temporal macula.[9,14] For direct comparison to these prior studies that analyze a smaller region within the retina, we repeated our analysis on the parafoveal regions between 500 and 1250 microns from the foveal center using binarized and skeletonized images (Supplementary Fig. S2), as well as binarized-only images (Supplementary Fig. S3). Despite these adjustments, our analysis did not demonstrate greater vessel density in the superior and inferior parafoveal regions.

There are several possible explanations for these different results. First, these studies used images obtained using different types of OCTA instruments. A comparison of the four major commercially available

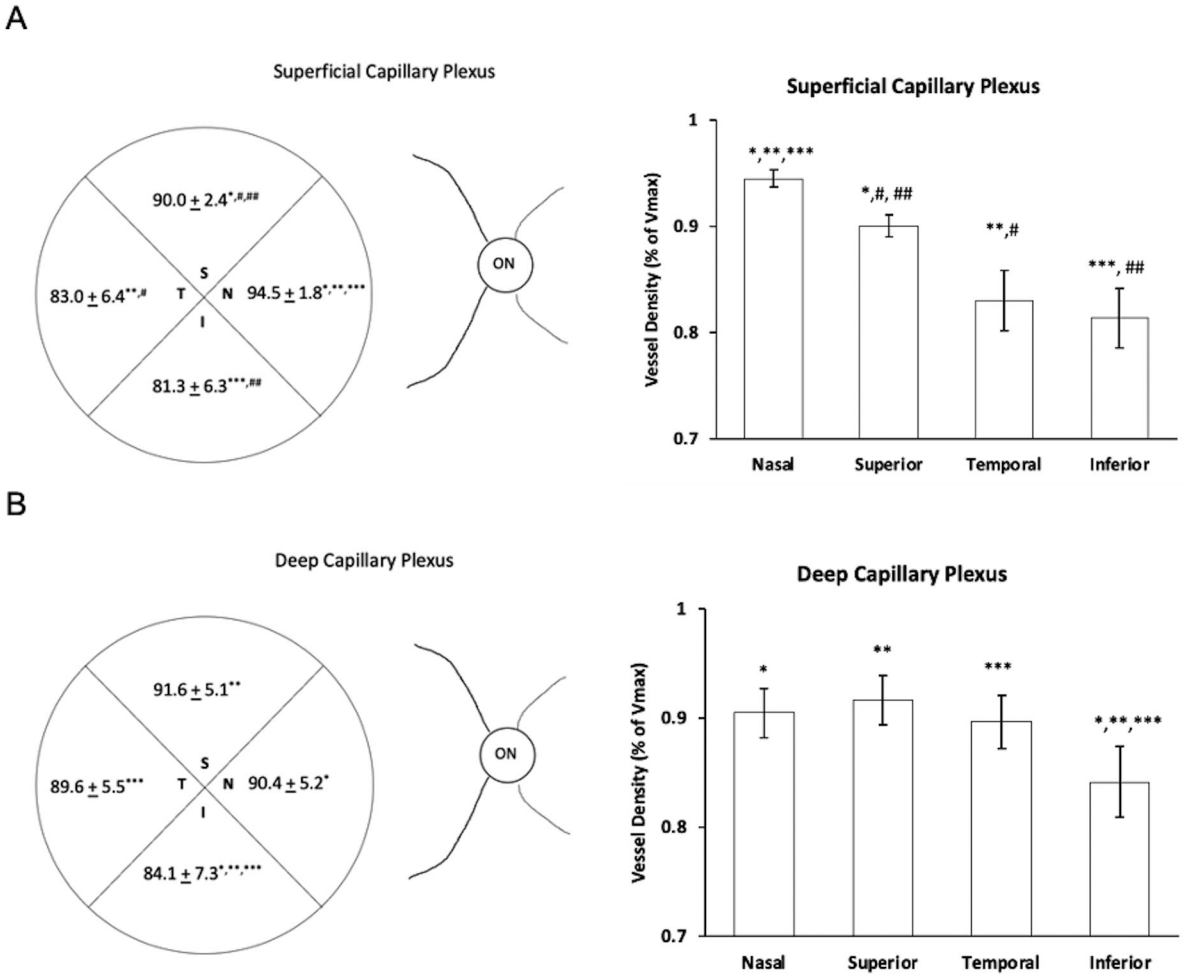

Figure 9. Quadrant analysis from a radius of 0 to 4000 microns. Vessel density of quadrants on skeletonized, binarized images for the (**A**) superficial capillary plexus and (**B**) deep capillary plexus. The nasal quadrant is defined as −45 to 45 degrees, the superior quadrant 45 to 135 degrees, temporal quadrant 135 to 225 degrees, inferior quadrant 225 to 315 degrees. (*Left*) The average vessel density (%) ± standard deviation is reported for each quadrant. (*Right*) The average vessel density (%) with a 95% CI is reported for each quadrant. I, inferior; N, nasal; ON, optic nerve; S, superior; T, temporal; Vmax, maximum vessel density. *Symbols* indicate statistically significant difference ($P < 0.05$) between the means.

OCTA revealed that the continuity of the vessels, as well as the overall reliability of the vessel imaging, was dependent on the imaging acquisition equipment.[26,27] Different methods of image processing, including image binarization, have also been shown to affect vessel density calculations.[28] These studies also employ different methods to estimate vessel density, with some relying on pixel density as a surrogate and others using fractal analysis.[9,14] Further studies are necessary to identify the most accurate OCTA imaging instrument, imaging processing technique, and vessel density calculation methodology.

OCTA studies evaluating vessel density of normal eyes have demonstrated that vessel density decreases with age. Iafe et al.[11] demonstrated that vessel density decreases by 0.26% per year at the superficial capillary plexus and 0.27% per year at the deep capillary plexus. In the present study, we use the normalized vessel density curves to eliminate the potential effect of age in our cohort. Instead of reporting the absolute vessel density, which may be affected by age, we report individuals' vessel density as a percentage of their own maximum vessel density. This process effectively allows each eye to serve as its own control and allows for a refined analysis of the topographic trend in vessel density while accounting for potential differences in the absolute vessel density between different eyes. Another advantage of the present study is the use of OCTA images that are both binarized and skeletonized. While previous studies mostly use binarized OCTA images, the major advantage of using skeletonized images is that the skeletonization process reduces the

overestimation of vessel density that occurs when larger vessels are included, as larger-caliber vessels do not play a direct role in gas exchange.[11]

There are several limitations to our study. Image artifacts, motion artifacts, and segmentation errors are commonly reported artifacts in OCTA imaging.[29] For example, overlying superficial vessels may cast a shadow on deeper layers, including the deep plexus, and artificially lower the vessel density calculation at these areas, a process known as negative projection. Our study also exclusively used images obtained on the Zeiss Cirrus OCTA, which has been reported to provide superior vessel imaging at the more superficial vascular layers but does not provide the definition of the Swept Source OCTA at the deeper vasculature beneath the retinal pigment epithelium.[27,30–32] For this reason, we analyzed the retinal vasculature and omitted the choriocapillaris layer. The present study also uses 8-mm × 8-mm images to establish topographic trends over a larger area of the posterior vasculature; however, these images have lower resolution compared to 3-mm × 3-mm and 6-mm × 6-mm images. Other limitations of the study include the retrospective nature of the study and the relatively small sample size.

In conclusion, our study provides a normative, continuous vessel density topography map of the retinal vasculature. The present study uses binarized and skeletonized OCTA images, which have been established as an effective and histologically accurate method of imaging blood vessels.[11,28] Our continuous vessel density analysis offers greater sensitivity in detecting topographic variations in vessel density compared to traditional methods of analysis, which report vessel density in discrete regions of the retina. This continuous vessel density topography analysis may serve as a normative database to better understand the vascular changes that occur in different chorioretinal diseases.

Acknowledgments

Disclosure: **M.M. Park**, None; **B.K. Young**, None; **L.L. Shen**, None; **R.A. Adelman**, None; **L.V.D. Priore**, Astellas Institute for Regenerative Medicine (C), LambdaVision (C), Tissue Regeneration Sciences (C), CavTheRx (C)

References

1. Cholkar K, Dasari SR, Pal D. Eye: anatomy, physiology and barriers to drug delivery. In: Mitra AK, ed. *Ocular Transporters and Receptors*. Sawston, United Kingdom: Elsevier; 2013:1–36.
2. Goldberg MF. Natural history of untreated proliferative sickle retinopathy. *Arch Ophthalmol*. 1971;85:428–437.
3. Hussnain SA, Coady PA, Slade MD, et al. Hemoglobin level and macular thinning in sickle cell disease. *Clin Ophthalmol (Auckland, NZ)*. 2019;13:627.
4. Marmor MF, Carr RE, Easterbrook M, Farjo AA, Mieler WF. Recommendations on screening for chloroquine and hydroxychloroquine retinopathy: a report by the American Academy of Ophthalmology. *Ophthalmology*. 2002;109:1377–1382.
5. Novotny HR, Alvis DL. A method of photographing fluorescence in circulating blood in the human retina. *Circulation*. 1961;24:82–86.
6. Agemy SA, Scripsema NK, Shah CM, et al. Retinal vascular perfusion density mapping using optical coherence tomography angiography in normals and diabetic retinopathy patients. *Retina*. 2015;35:2353–2363.
7. Al-Sheikh M, Akil H, Pfau M, Sadda SR. Swept-source OCT angiography imaging of the foveal avascular zone and macular capillary network density in diabetic retinopathy. *Invest Ophthalmol Vis Sci*. 2016;57:3907–3913.
8. Al-Sheikh M, Tepelus TC, Nazikyan T, Sadda SR. Repeatability of automated vessel density measurements using optical coherence tomography angiography. *Br J Ophthalmol*. 2017;101:449–452.
9. Coscas F, Sellam A, Glacet-Bernard A, et al. Normative data for vascular density in superficial and deep capillary plexuses of healthy adults assessed by optical coherence tomography angiography. *Invest Ophthalmol Vis Sci*. 2016;57:OCT211–OCT223.
10. Durbin MK, An L, Shemonski ND, et al. Quantification of retinal microvascular density in optical coherence tomographic angiography images in diabetic retinopathy. *JAMA Ophthalmol*. 2017;135:370–376.
11. Iafe NA, Phasukkijwatana N, Chen X, Sarraf D. Retinal capillary density and foveal avascular zone area are age-dependent: quantitative analysis using optical coherence tomography angiography. *Invest Ophthalmol Vis Sci*. 2016;57:5780–5787.
12. Wang Q, Chan S, Yang JY, et al. Vascular density in retina and choriocapillaris as measured by optical coherence tomography angiography. *Am J Ophthalmol*. 2016;168:95–109.
13. You QS, Wang J, Guo Y, et al. Detection of reduced retinal vessel density in eyes with geographic atrophy secondary to age-related macular

degeneration using projection-resolved optical coherence tomography angiography. *Am J Ophthalmol*. 2020;209:206–212.
14. Gadde SG, Anegondi N, Bhanushali D, et al. Quantification of vessel density in retinal optical coherence tomography angiography images using local fractal dimension. *Invest Ophthalmol Vis Sci*. 2016;57:246–252.
15. Takayama K, Kaneko H, Ito Y, et al. Novel classification of early-stage systemic hypertensive changes in human retina based on OCTA measurement of choriocapillaris. *Sci Rep*. 2018;8:1–13.
16. Rosenfeld PJ, Durbin MK, Roisman L, et al. ZEISS Angioplex spectral domain optical coherence tomography angiography: technical aspects. In: Bandello F, Souied EH, Querques G, eds. *OCT Angiography in Retinal and Macular Diseases*. Basel, Switzerland: Karger Publishers; 2016:18–29.
17. Nassisi M, Baghdasaryan E, Tepelus T, Asanad S, Borrelli E, Sadda SR. Topographic distribution of choriocapillaris flow deficits in healthy eyes. *PLoS One*. 2018;13:e0207638.
18. Al-Sheikh M, Phasukkijwatana N, Dolz-Marco R, et al. Quantitative OCT angiography of the retinal microvasculature and the choriocapillaris in myopic eyes. *Invest Ophthalmol Vis Sci*. 2017;58:2063–2069.
19. Phansalkar N, More S, Sabale A, Joshi M. Adaptive local thresholding for detection of nuclei in diversity stained cytology images. In: *2011 International Conference on Communications and Signal Processing*. Kerala, India: IEEE; 2011:218–220.
20. Spaide RF. Choriocapillaris flow features follow a power law distribution: implications for characterization and mechanisms of disease progression. *Am J Ophthalmol*. 2016;170:58–67.
21. Uji A, Balasubramanian S, Lei J, Baghdasaryan E, Al-Sheikh M, Sadda SR. Choriocapillaris imaging using multiple en face optical coherence tomography angiography image averaging. *JAMA Ophthalmol*. 2017;135:1197–1204.
22. Muggeo VM, Atkins DC, Gallop RJ, Dimidjian S. Segmented mixed models with random changepoints: a maximum likelihood approach with application to treatment for depression study. *Stat Model*. 2014;14:293–313.
23. Spaide RF, Klancnik JM, Cooney MJ. Retinal vascular layers imaged by fluorescein angiography and optical coherence tomography angiography. *JAMA Ophthalmol*. 2015;133:45–50.
24. Stanga PE, Lim JI, Hamilton P. Indocyanine green angiography in chorioretinal diseases: indications and interpretation: an evidence-based update. *Ophthalmology*. 2003;110:15–21.
25. Shahlaee A, Pefkianaki M, Hsu J, Ho AC. Measurement of foveal avascular zone dimensions and its reliability in healthy eyes using optical coherence tomography angiography. *Am J Ophthalmol*. 2016;161:50–55.e51.
26. De Vitis LA, Benatti L, Tomasso L, et al. Comparison of the performance of two different spectral-domain optical coherence tomography angiography devices in clinical practice. *Ophthalmic Res*. 2016;56:155–162.
27. Munk MR, Giannakaki-Zimmermann H, Berger L, et al. OCT-angiography: a qualitative and quantitative comparison of 4 OCT-A devices. *PLoS One*. 2017;12:e0177159.
28. Mehta N, Liu K, Alibhai AY, et al. Impact of binarization thresholding and brightness/contrast adjustment methodology on optical coherence tomography angiography image quantification. *Am J Ophthalmol*. 2019;205:54–65.
29. Spaide RF, Fujimoto JG, Waheed NK. Image artifacts in optical coherence angiography. *Retina (Philadelphia, Pa)*. 2015;35:2163.
30. Miller AR, Roisman L, Zhang Q, et al. Comparison between spectral-domain and swept-source optical coherence tomography angiographic imaging of choroidal neovascularization. *Invest Ophthalmol Vis Sci*. 2017;58:1499–1505.
31. Novais EA, Adhi M, Moult EM, et al. Choroidal neovascularization analyzed on ultrahigh-speed swept-source optical coherence tomography angiography compared to spectral-domain optical coherence tomography angiography. *Am J Ophthalmol*. 2016;164:80–88.
32. Waheed NK, Moult EM, Fujimoto JG, Rosenfeld PJ. Optical coherence tomography angiography of dry age-related macular degeneration. In: Bandello F, Souied EH, Querques G, eds. *OCT Angiography in Retinal and Macular Diseases*. Basel, Switzerland: Karger Publishers; 2016:91–100.